Shape Analysis of Corpus Callosum in Autism Subtype using Planar Conformal Mapping

Qing He[*1], Ye Duan[1], Xiaotian Yin[2], Xianfeng Gu[2], Kevin Karsch[1], Judith Miles[3]
[1] Department of Computer Science, University of Missouri-Columbia, Columbia, MO, USA 65211
[2] State University of New York at Stony Brook, Stony Brook, New York, USA 11794
[3] Thompson Center for Autism, University of Missouri-Columbia, Columbia, MO, USA 65211

ABSTRACT

A number of studies have documented that autism has a neurobiological basis, but the anatomical extent of these neurobiological abnormalities is largely unknown. In this study, we aimed at analyzing highly localized shape abnormalities of the corpus callosum in a homogeneous group of autism children. Thirty patients with essential autism and twenty-four controls participated in this study. 2D contours of the corpus callosum were extracted from MR images by a semiautomatic segmentation method, and the 3D model was constructed by stacking the contours. The resulting 3D model had two openings at the ends, thus a new conformal parameterization for high genus surfaces was applied in our shape analysis work, which mapped each surface onto a planar domain. Surface matching among different individual meshes was achieved by re-triangulating each mesh according to a template surface. Statistical shape analysis was used to compare the 3D shapes point by point between patients with autism and their controls. The results revealed significant abnormalities in the anterior most and anterior body in essential autism group.

Keywords: Corpus callosum, autism, shape analysis, planar conformal mapping

1. INTRODUCTION

Autism is a spectrum of complex neurodevelopmental disorders of childhood defined by the presence of social deficits, abnormalities in communication, the presence of stereotyped, repetitive behaviors, and a characteristic course. Despite the large number of structural imaging studies in autism, results are generally inconclusive, and sometimes even contradictory. The corpus calllosum (CC) is the major commissural pathway between the brain hemispheres and plays an integral role in relaying sensory, motor, and cognitive information from homologous regions in the two hemispheres. Several studies have reported deficits in the size of the corpus callosum (CC) and its subregions, although the results are inconsistent with regard to CC sub-regions. For example, [2] reported reductions in the size of the body and posterior regions of the CC in autistic patients, [7] found significant differences in anterior regions, and [1] found reductions in genu and splenium as well as the total CC area. One possible reason for the inconsistency is that heterogeneity within the autism diagnosis obscures the genetic basis of the disorder [5]. Recently, Miles et al. proposed a new definition of autism subgroups, which divided autism into essential autism and complex autism [5]. Limiting studies of brain morphology to individuals with essential autism decreases the background noise of structural variation and allow the analysis of the more uniform population. He et.al [16] first adopted this definition and compared the shape difference between subjects with essential autism and controls, although their sample size was conspicuously small. In this paper, we also focus on essential autism.

Quantitative morphologic assessment of individual brain structures is often based on volumetric measurements and shape analysis. Shape analysis has gained an increasing amount of interest from the neuroimaging community because it can precisely locate morphological changes in pathological structures, which cannot be reflected in volume measurements. Shape morphology of the CC in autism has been studied in [1] and [16]. In [1], CC thickness (the distance from a medial line) at each surface point was compared between patients and controls. In [16], an average CC model was used as a template and the distance to the template at each point was compared between two groups.

[*] qhgb2@mizzou.edu; phone: 1 573 882 3951

Medical Imaging 2009: Biomedical Applications in Molecular, Structural, and Functional Imaging, edited by Xiaoping P. Hu, Anne V. Clough, Proc. of SPIE Vol. 7262, 726217 · © 2009 SPIE · CCC code: 1605-7422/09/$18 · doi: 10.1117/12.812285

However, the shape analysis in both was still in a 2D fashion, because the comparison was performed on a contour-by-contour basis.

This paper analyzes the 3D shape morphology of the CC in essential autism. The 3D model of the CC is reconstructed from 2D contours of nine sagittal slices. A semiautomatic segmentation method is used for 2D segmentation on each slice. In the shape analysis we directly compare the 3D coordinates at each surface point of the CC model using Hotelling T^2 two sample tests. In order to perform this comparison, point correspondence among different individual models must be established. We develop a new planar conformal mapping to map the surface onto a planar domain and thus find a one-to-one point correspondence among different models.

Conformal parameterization has been explored intensively as a potential approach to the matching and analysis of brain data. It maps the brain surface into regular and simpler domain and carries out the analysis on the parameter domain. [8] used spherical conformal map to match cortical surfaces, where they parameterize the genus zero closed surfaces by spheres. Based on the shape characteristics of the two structures, we design a conformal method to parameterize the target surfaces with a planar domain and then match the points among them.

2. MATERIALS AND METHODS

2.1 Subjects and data

Thirty patients with essential autism participated in this study. The mean age of the patients was 8.5 (range 3-18). All patients met the DSM-IV criteria [10] as well as Autism Diagnostic Interview-Revised (ADI-R) and ADOS algorithm criteria. The distinction between essential and complex autism is based on the presence of generalized dysmorphology which is indicative of an insult to early embryologic development and has been previously reported [5]. Children with a known disorder such as Fragile X, Tuberous Sclerosis, a chromosome abnormality or severe prematurity with brain damage and children with IQs/DQs less than 40 will be excluded. Five healthy patients recruited from the NIH Human Brain Project with matched ages (range 4-19) participated as controls. Besides, we also obtained MR images of nineteen normal people (age range 15-30) from IBSR database [15]. Both groups include males and females at roughly equal number.

MR images of our patients and controls were obtained from our autism aesthesia protocol which included intravenous infusion of protocol to insure image quality. Axial, coronal and sagittal T1-weighted images were acquired using the Siemens Symphony 1.5 T scanner with the following parameters: TR = 35ms, NEX = 1, flip-angle = 30 degrees, thickness = 1.5mm, field of view = 22cm, matrix =512x512. The data obtained from IBSR were T1-weighted MR images with 3.1mm thickness. Each brain volume was resampled with 1-mm isotropic voxels to balance between computational cost and data quality.

2.2 CC modeling

We start with slice-by-slice segmentation and stack the 2D curves to make a 3D model. Because it is more straightforward to verify the accuracy of 2D results slice by slice, this method provides better results as opposed to direct 3D segmentation and validation. From the sagittal planes, the midsagittal section that most clearly displays the cerebral aqueduct, CC, and superior colliculus, is selected manually [23]. Mid-sagittal slice and four adjacent slices on each side are used for CC segmentation. On each slice, the CC is segmented using a semiautomatic method described in [9]. The user initializes a polyline inside the CC region by three mouse clicks (Fig. 1(a)), and a seed contour consisting of four parts is automatically generated by point tracing on the edge map (Fig. 1(b), (c)). The seed will then automatically deform according to active contour evolution, but each part has its own motion law. The fornix tip can also be removed by automatic fornix detection [9]. In order to ensure the accuracy of the segmentation, we allow manual adjustment of the segmentation result if it did not comply with the true CC boundary. Generally this method works well on most data sets, and the need for manual adjustment is rare. The resulting contour is represented as a sequential point list and its visualization is shown in Fig. 1(d).

Contour stitching is performed to create the 3D CC model of each subject. Since the segmentation method can keep track of the four parts of the CC boundary, the point correspondence problem can be simplified by first matching the sensor points among contours [16]. After matching the sensor points, the four parts are implicitly matched among contours. We only need to match the individual points within each part. The details of matching the sensor points and the inner points of the four parts can be found in [16]. By connecting the matched point pairs between adjacent contours, the

3D mesh is created. A tangential Laplacian smoothing [17] is performed to maintain a good node distribution of the model. The reconstructed model is shown in Fig. 2. The inner side of the surface is rendered in green in this figure.

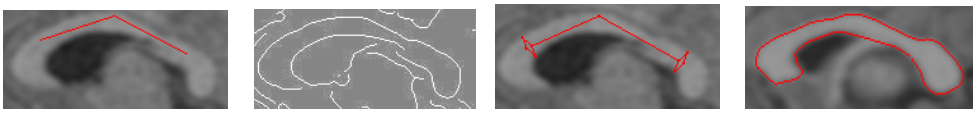

(a) (b) (c) (d)

Fig. 1. (a) User-initialized polyline. (b) The edge map. (c) The completed seed contour. (d) The final result

2.3 Surface correspondence

Conformal parameterization has been explored intensively as a potential approach to the matching and analysis of brain data. It maps the brain surface into regular and simpler domains and carries out the analysis on the parameter domain. [19] used spherical conformal map to match cortical surfaces, where they parameterized the genus zero closed surfaces by spheres. Unlike their data, the CC surfaces we are studying have two boundaries which are the 2D CC contours of the two end slices. Inspired by [18], we design a planar conformal mapping method. In order to find point correspondence among difference CC surfaces, we first parameterize each CC surface using a planar domain, and then align the parameterization in the planar domain so that surface points across different objects posses the same parameterization. Finally, the aligned parameterization in the planar domain is mapped back onto the original surfaces (Fig. 2).

Among all the CC models an arbitrary model is chosen as the target surface, and the corresponding points on the other models (source surfaces) are to be established to match the points on the target surface. We conformally flatten the target surface *M* onto a planar domain *M'*, which is a rectangle with the two boundaries γ_1 and γ_2 mapped to the upper and lower long edges. In order to parameterize the given surface with a planar domain, we need to construct a special holomorphic one-form $\tau + \eta\sqrt{-1}$, such that its integration around the boundaries has a real part with a constant period, while the integration along a path from one boundary to the other has a constant imaginary part. To get the imaginary part η, we need to compute a harmonic function f by solving a Dirichlet problem:

$$\begin{aligned} \Delta f &= 0, \\ f|_{\gamma_1} &= 1, \\ f|_{\gamma_2} &= 0. \end{aligned} \qquad (1)$$

η is the gradient of *f*, and the real part τ is the conjugate of η. In our implementation, we first convert η into a piece-wise constant vector field υ_η sampled at each face; rotate υ_η by 90° around the face normal, and turn the rotated vector field into the one-form τ. Choosing an appropriate starting point, we can integrate the holomorphic one-form $\tau + \eta\sqrt{-1}$ on *M*. Taking the real and imaginary parts of the integration to be y and x coordinates respectively, we get a horizontal strip which is periodic along the X direction. Cutting the strip along the vertical line *x=0*, we get the final planar domain *M'*, where the upper and lower side corresponds to the two boundaries in the original mesh *M*. The map from *M* to *M'* is conformal; the height-width ratio of the rectangle is a conformal invariant of the original surface. In our experiments, we always rescale the rectangle uniformly along the X and Y directions so that the width equals 2π. As a consequence, the intrinsic structure is solely reflected by the height of the rectangle for our cases.

The same method is used to map each source surface onto its planar domain. After that, we compute the map between the target planar domain and each source planar domain. In our case, a reasonable map should satisfy two constraints. First, each boundary of the source surface should be aligned with the corresponding boundary of the target surface. In the rectangle domain, we need to map the upper (lower) edge of the source rectangle to the upper (lower) side of the target rectangle. As mentioned before, the width of the rectangle is always equal to 2π, while the height may be different from model to model. Therefore we may need to rescale one rectangle along Y direction to align with the other rectangle. In our experiments, all the rectangles have similar heights, so the rescaling factor is very close to one and

therefore would not hurt the conformality of the map too much. Even in the case of a bigger rescaling factor, the map is still affine and therefore harmonic, which is already strong enough for our purpose. The second constraint is to align the "bending corner" (i.e. posterior angle of genu) across two surfaces. In order to make the mapping process easier, we choose the bending corner to be the starting point used in the integration of the holomorphic one-form. As a consequence, in the planar domain the bending corner will appear at the vertical cutting side. Aligning the two rectangles along their left and right sides, the bending corners will be automatically matched. Since all the rectangles have the same width 2π, we do not need to rescale any of them along X direction.

Once the source rectangle is totally aligned with the target one, we get a map *F'* between two planar domains. For each vertex *v* on the target rectangle, there is a point *F'(v)* in the source rectangle, which may lie inside a triangle, on an edge or at a vertex. Without loss of generality, we represent the point as a linear combination $F'(v) = b_0 v_0 + b_1 v_1 + b_2 v_2$, where v_i is the vertex of the resident face and b_i the corresponding barycentric coordinate. The map *F'* between two planar domains induces a map *F* between the two original surfaces. Namely, each vertex v in the target surface corresponds to a point $F(v) = b_0 v_0 + b_1 v_1 + b_2 v_2$ in the source surface. To facilitate later processing, we resample the source surface using these points as vertices, and re-triangulate the source surface with the same connectivity as that of the target surface. Therefore, each point on the source surface has a correspondence on the target surface, and the two surfaces have the same triangulation.

The same method is used to align each source planar domain to the target planar domain, and to re-triangulate the source surface. In this way, the point correspondence among all the surfaces is established through the target surface.

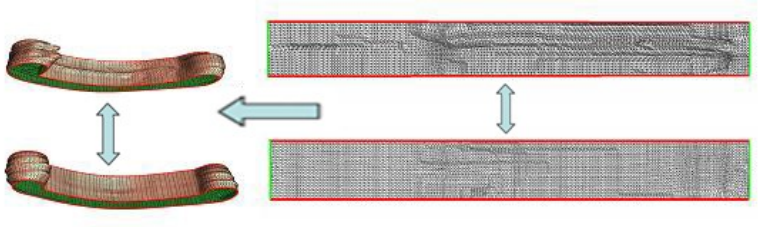

Fig. 2. Illustration of establishing point correspondence via planar conformal mapping: two individual CC models (left) and their planar domains (right)

2.4 Statistical shape analysis

Before the shape analysis, rigid-body Procrustes Analysis [11] is performed on each 3D mesh across subjects. The details of the algorithm can be found in [11]. In the local shape analysis, difference between groups at every surface location is tested. The difference in the size of the CC has been eliminated in the spatial alignment, so the shape analysis only reveals pure shape difference between patients and controls. This can be done in two main fashions [16]. One way is to analyze the local difference to a template, which is usually the mean of the two groups. Student t-test can be used to test the local significance and [2] used this method. The main disadvantage of this method is the need to select a template, which introduces an additional bias. The other method is to directly analyze the spatial location of each point, and we apply this method in our study. No template is needed in this approach and multivariate statistics of the (x,y,z) location is used. Hotelling T^2 two-sample metric is used to measure how two groups are locally different from each other. We use a modified T^2 metric instead of the standard one, because it is less sensitive to group differences of the covariance matrixes and the sample size [16]. This metric is defined as

$$T^2 = (\mu_1 - \mu_2)'((1/n_1)\Sigma_1 + (1/n_2)\Sigma_2))^{-1}(\mu_1 - \mu_2) \qquad (2)$$

where Σ_1, Σ_2 are the covariance matrixes of the two groups, μ_1, μ_2 are the average coordinates of the two groups at this surface point, and n_1, n_2 are the sample sizes of the two groups. A positive, larger T^2 indicates more significant group difference, and each T^2 is converted to a corresponding p-value at every surface location. This raw p-value is an

optimistic estimation. Since comparisons are made at thousands of CC surface points, it is important to control for the multiple testing problem. There are several methods to deal with multiple comparison problem, such as random field [21, 22], non-parametric permutation test [20] and false discovery rate estimation (FDR) [6]. In our work, we adopt FDR as the appropriate approach for p-value correction, because it provides an interpretable and adaptive criterion, while non-parametric permutation tests are overly pessimistic [6]. FDR method allows the false positive to be within a small proportion α (α =0.01 in our experiment). The p-value correction is computed as follows [6].

1. Sort the p-values such that $p_1 < p_2 < \ldots < p_N$, where N is the number of vertices on the surface.
2. From all the p-values that satisfy $p_i <= \alpha \bullet i/N$, select the p-value with the largest index i, denoted as p_{α}.
3. Declare all locations with p-values less than p_{α} significant.

Both raw and corrected p values are shown in the experiment. A schematic view of our statistical analysis procedure can be seen in Fig. 3.

We also perform a global shape analysis, where the average of the local Hotelling T^2 metrics across the whole surface is calculated for each subject, and the p-value is computed the same way as for the local testing. No permutation is needed since there is only one test.

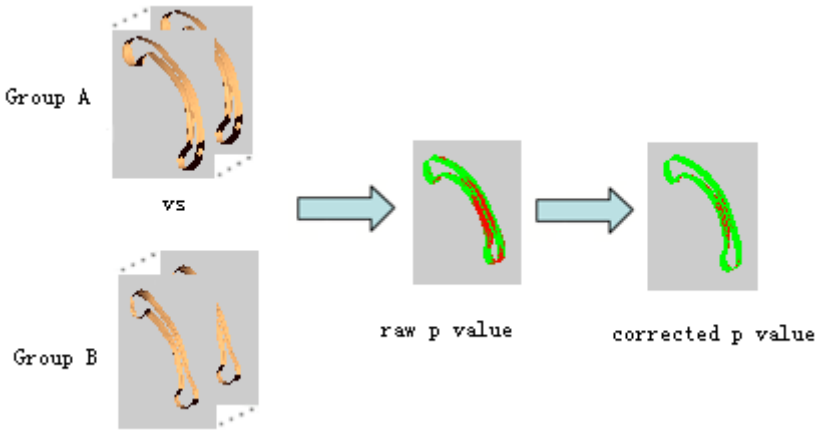

Fig. 3. Schematic view of the test procedure

3. RESULTS AND DISCUSSION

3.1 Group mean difference map

Fig. 4 gives a descriptive visualization of the group difference. The overlaid average CC structures are shown in Fig. 4(a). Fig. 4(b) shows the signed distance map between the two average structures rendered on an overall average shape, where the negative distances indicate the patients' structure is outside the controls' and the reverse is for the positive distances. In the patients' structure, the anterior most is more projected, both anterior bottom and posterior bottom are less downward, the anterior body is thicker and the posterior body (including isthmus) is thinner.

Fig. 4. (a) Overlaid average structures (blue: controls, red: patients) (b) Distance map between the two averages

3.2 Local shape difference map

The significance maps of the raw and corrected p-values are shown as color coded p-values in Fig. 5. Smaller p-values indicate larger statistical significance. A one-tailed alpha level of 0.05 is chosen as the significance threshold. Fig. 5(a) is the significance map of raw p-values, which reveals significant difference in the anterior most, anterior body and posterior top. The corrected significance map after FDR is shown in Fig. 5(b), which retains a small portion of significant difference in the anterior most and anterior body, while the difference in the posterior top has no significance. The global shape analysis has a p value of 0.008 which indicates there is significant difference in the overall shape of the CC between patients and controls.

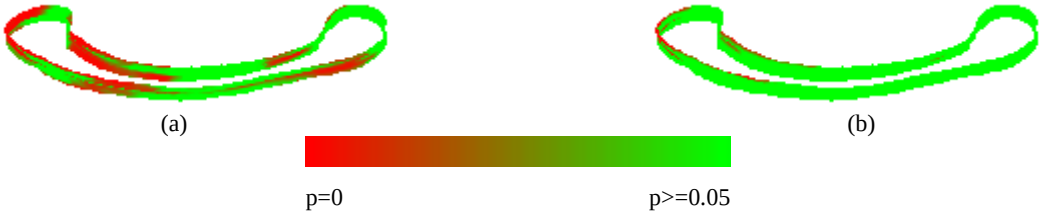

Fig. 5. Significance map: (a) raw p values (b) corrected p values

3.3 Discussion

From the descriptive visualization, we find flattened anterior and posterior parts, thickened anterior body and thinned posterior body. The raw significance map suggests significant differences in the anterior most, anterior body and posterior top, while the corrected significance map only retains the significance in the anterior most and anterior body. We compare our findings with two most relevant studies [1, 16]. Table 1 gives a summary of the findings in [1], [16] and our study regarding the shape differences between autism and control groups. Both [1] and [16] found less arching in the body of the CC, but our result is different from theirs. [1] and [16] showed opposite results in anterior and posterior parts. However, the results in [16] did not show any significance in these parts, so its conclusion may be accidental due to small sample size. Another possible reason for this inconsistency is that the subjects were from essential autism group in [16] instead of the whole autism group in [1]. Our study also focuses on essential autism and finds the same result with [16] in the anterior part. Our result further shows significant difference between patients and controls in this part, which may indicate a feature exclusively for essential autism. Our result for posterior part is not similar to either [1] or [16], and it does not show any significance either. This may indicate that there is no special pattern in the posterior of the CC in essential autism, but there is a pattern in this part in the whole autism group.

The results of this study need to be interpreted cautiously because of several limitations. First of all, the age range of the population is large, so the effect of the brain size on the CC shape may be significant. We have removed the size effect during Procrustes alignment, which leads to a pure shape comparison in our results. Therefore, our results may still be justified, but further test with the brain size as a covariate is necessary to confirm the results. Secondly, we exclude the complex autism group as it was done in [16], but our results show some inconsistency with [16]. This may be due to the different sample size, population age, and methodology in the two studies. Further studies on different subgroups within autistic patients need to be done, such as male vs. female, and complex vs. essential. These findings will better explain the inconsistent results caused by the population.

Table 1 Comparison of three studies

CC regions	Body		Anterior		Posterior	
	Shape	Significant	Shape	Significant	Shape	Significant
[1]	Less arching	No	More inward	Yes	More inward	Yes
[16]	Less arching	Yes	More projected	No	More projected	No
Our study	Posterior thin	No	More projected	Yes	Less downward	No
	Anterior thick	Yes				

4. CONCLUSION

Based on the new definition of autism subgroups, we investigate the CC abnormalities in essential autism, and exclude the complex autism group in order to find more homogeneous results. We use a semiautomatic method to segment 2D CC boundaries, and 3D surfaces are reconstructed by contour stitching. A newly developed planar conformal mapping is used to parameterize the 3D surfaces. Shape comparison is conducted at each surface location using Hotelling T^2 test followed by p-value correction using FDR. We have found significant shape difference in the anterior most and anterior body of the CC between patients and controls. The results may provide some insights into clinical diagnosis, but further studies are necessary to validate the results.

ACKNOWLEDGEMENTS

This work is supported in part by a NIH pre-doctoral training grant for Clinical Biodetectives, Thompson Center Research Scholar fund, Department of Defense Autism Concept Award, NARSAD Foundation Young Investigator Award.

REFERENCES

[1] C. N. Vidal, R. Nicolson, T. J. DeVito, K. M. Hayashi, J. A. Geaga, D. J. Drost, P. C. Williamson, N.Rajakumar, Y. Sui, R. A. Dutton, A.W. Toga, and P.M. Thompson, Mapping corpus callosum deficits in autism: an index of aberrant cortical connectivity, Biological Psychiatry, 60(3), 2006, pp. 218-225.

[2] J. Piven, J. Bailey, B. J. Ranson, and S. Arndt, An MRI study of the corpus callosum in autism, Am J Psychiatry, 154, 1997, pp. 1051-1056.

[3] S. L. Palmer, W. E. Reddick, J. O. Glass, A.Gajjar, O. Goloubeva, and R. K. Mulhern, Decline in corpus callosum volume among pediatric patients with medulloblastoma: longitudinal MR imaging study, AJNR Am J Neuroradiol, 23, 2002, pp. 1088–1094

[4] R. Nicolson, T.J. Devito, C.N. Vidal, Y. Sui, K.M. Hayashi, D.J. Drost, P.C. Williamson, N. Rajakumar, A.W. Toga, and P.M. Thompson, Detection and mapping of hippocampal abnormalities in autism, Psychiatry Research: Neuroimaging, 148, 2006, pp. 11-21

[5] J.H. Miles, T.N. Takahashi, S. Bagby, P.K. Sahota, D.F. Vaslow, C.H. Wang, R.E. Hillman, and J.E. Farmer, Essential vs Complex Autism: Definition of Fundamental Prognostic Subtypes, Am. J. Medical Genetics, 135A, 2005, pp.171-180

[6] M. Styner, L. Oguz, S. Xu, C. Brechbuehler, D. Pantazis, J.J. Levitt, M.E. Shenton, and G. Gerig, Framework for the Statistical Shape Analysis of Brain Structures using SPHARM-PDM, ISC/NA-MIC Workshop on Open Science at MICCAI, 2006

[7] A.Y. Hardan, N.J. Minshew, and M.S. Keshavan, Corpus callosum size in autism, Neurology, 55, 2000, pp. 1033–1036

[8] P. Brambilla, A. Hardan, S. Ucelli di Nemi, J. Perez, J.C. Soares, and F. Barale, Brain anatomy and development in autism: review of MRI studies, Brain Research Bulletin, 61, 2003, pp. 557-569

[9] Q. He, Y. Duan, JH. Miles, N. Takahashi, A Context-Sensitive Active Contour for Image Segmentation, International Journal of Biomedical Imaging, vol. 2007, Article ID 24826, 8 pages, 2007. doi: 10.1155/2007/24826

[10] American Psychiatric Association, Diagnostic and Statistical Manual of Mental Disorders, 4th ed., text revision, American Psychiatric Association, Washington DC, 2000

[11] Amy Ross, Procrustes analysis, Technical Report, Department of Computer Science and Engineering, University of South Carolina, SC 29208, www.cse.sc.edu/~songwang/CourseProj/proj2004/ross/ross.pdf

[12] T. McInerney, G. Hamarneh, M. Shenton, and D. Terzopoulos, Deformable organisms for automatic medical image analysis, Medical Image Analysis, 6, 2002, pp. 251-266

[13] L. Liu, G. Wang, B. Zhang, B. Guo, and H.Y. Shum, Perceptually based approach for planar shape morphing, Proceedings of the 12th Pacific Conference on Computer Graphics and Applications, 00, 2004, pp. 111 – 120
[14] Pahal Dalal, Brent C.Munsell, Song Wang, Jijun Tang, Kenton Oliver, A fast 3D correspondence method for statistical shape modeling, IEEE Conference on Computer Vision and Pattern Recognition, 2007. 17-22 June 2007, pp:1 - 8
[15] http://www.cma.mgh.harvard.edu/ibsr/
[16] Q. He, Y. Duan, JH. Miles, TN. Takahashi, Statistical Shape Analysis of the Corpus Callosum in Subtypes of Autism, IEEE 7th International Symposium on Bioinformatics & Bioengineering, Boston, Massachusetts, USA, Oct 14-17, 2007
[17] Z. Wood, M. Desbrun, P. Schroder, and D. Breen, Semi-Regular Mesh Extraction from Volume, Proceedings of the conference on Visualization, 2000: 275 - 282
[18] X. Gu and S. Yau, Global conformal surface parameterization, in Proc. ACM Symp. Geometry Processing, 2003, pp. 127–137.
[19] Xianfeng Gu, Yalin Wang, Tony F. Chan, Paul M. Thompson, and Shing-Tung Yau. Genus Zero Surface Conformal Mapping and Its Application to Brain Surface Mapping. IEEE TRANSACTIONS ON MEDICAL IMAGING, 23(8), 2004
[20] D. Pantazis, R.M. Leahy, T.E. Nichol, and M. Styner, Statistical surface-based morphometry using a non-parametric approach, Int. Symposium on Biomedical Imaging(ISBI), April 2004, pp. 1283–1286. 2.1, 2.6
[21] M. K. Chung, Statistical Morphometry in Neuroanatomy, Ph.D. thesis, McGill University, Montreal, 2001. 2.6
[22] K. J. Worsley, S. Marrett, P. Neelin, A. C. Vandal, K. J. Friston, and A. C. Evans, A unified statistical approach for determining significant signals in images of cerebral activation, Human Brain Mapping, vol. 4, pp. 58–73, 1996. 2.6
[23] Ozdemir ST, Ercan I, Sevinc O, Guney I, Ocakoglu G, Aslan E, Barut C. Statistical shape analysis of differences in the shape of the corpus callosum between genders, the anatomical record, 2007, 290:825-830.